Journal of Nuclear Medicine, published on June 13, 2017 as doi:10.2967/jnumed.117.191049

Optimization of SPECT Measurement of Myocardial Blood Flow with Corrections for Attenuation, Motion, and Blood-Binding Compared to PET

R Glenn Wells[1], Brian Marvin[1], Marlie Poirier[1], Jennifer Renaud[1], Robert A deKemp[1], Terrence D Ruddy[1]

[1]Division of Cardiology, University of Ottawa Heart Institute, Ottawa, ON Canada

Funding Support: Study was supported by a grant from GE Healthcare.

Disclosures: RG Wells and TD Ruddy have received research grant support from GE Healthcare. RA deKemp and J Renaud receive license revenues from the sale of FlowQuant™ and consult with Jubilant DraxImage Inc.

Corresponding (First) Author:

R. Glenn Wells
H1233, Cardiac PET Research
University of Ottawa Heart Institute
40 Ruskin St., Ottawa, ON, Canada, K1Y 4W7
Email: gwells@ottawaheart.ca
Phone: (613) 798-5555 x 18175
Fax: (613) 761-4929

Word Count: 4978

Running Title: Optimizing SPECT MBF vs PET

ABSTRACT

Myocardial blood flow (MBF) and flow reserve (MFR) measured with positron emission tomography (PET) have clinical value. Single-photon emission computed tomography (SPECT) cameras with solid-state detectors can obtain dynamic images for measurement of MBF and MFR. In this study, SPECT measurements of MBF made using ^{99m}Tc-tetrofosmin were compared to PET in the same patients. **Methods:** Thirty-one patients had PET MBF rest-stress studies performed with ^{82}Rb or ^{13}N- ammonia within one month of their SPECT. Dynamic rest-stress measurements were made using a SPECT camera. Kinetic parameters were calculated using a 1-tissue-compartment model and converted to MBF and MFR. Processing with and without corrections for attenuation (±AC), patient body motion (±MC) and binding of the tracer to red blood cells (±BB) was evaluated. **Results**: Both +BB and +MC improved the accuracy and precision of global SPECT MBF compared to PET MBF resulting in an average difference of 0.06 ± 0.37 mL/min/g. Global MBF and detection of abnormal MFR were not significantly improved with +AC. Global SPECT MFR with +MC and +BB had an area under the receiver operating curve (A_{ROC}) of 0.90 (+AC) to 0.95 (-AC) for detecting abnormal PET MFR < 2.0. Regional analysis produced similar results with an A_{ROC} of 0.84 (+AC) to 0.87 (-AC). **Conclusion**: Solid-state SPECT provides global MBF and MFR measurements that differ from PET by 2% ± 32% (MBF) and 2% ± 28% (MFR).

Key Words: SPECT myocardial blood flow, PET, attenuation correction, cadmium zinc telluride

INTRODUCTION

PET measurement of MBF and MFR has been shown to have incremental benefit over relative myocardial perfusion imaging (MPI) for diagnosis (*1-3*) and prognosis (*4-6*). However, while 6.4 million MPI studies are done annually in North America, <1% are done with PET (*7,8*). Measuring MBF is difficult with traditional SPECT cameras because of the limited sensitivity and lower temporal resolution compared to PET. Despite these challenges, dynamic acquisitions with rapid sequential rotations (*9*) and spline-based 4-dimensional reconstruction approaches (*10*) have demonstrated the potential for SPECT to provide accurate MBF measurements . The introduction of dedicated solid-state cardiac cameras greatly facilitates the acquisition protocol for dynamic SPECT imaging due to their improved sensitivity and temporal resolution (*11,12*). Animal studies comparing to microspheres have shown that these cameras can accurately measure MBF using either ^{201}Tl or ^{99m}Tc-based standard perfusion tracers (*13*). Human studies have shown that indices of flow correspond well with coronary angiography using sestamibi (*14*), tetrofosmin (*15*) and thallium (*16*). Recently, a SPECT flow index, measured using tetrofosmin, has shown good sensitivity (70%) and specificity (78%) for detecting abnormal flow as measured in the same patients with ammonia PET (*17*). To convert indices of flow into MBF, the flow-dependent extraction fraction for SPECT tracers in humans is needed.

We measured SPECT MBF with ^{99m}Tc-tetrofosmin, using a dedicated cardiac SPECT camera and a Renkin-Crone model for the extraction fraction, and evaluated the incremental value of corrections for body motion, blood-binding and attenuation against PET MBF measured in the same patients.

METHODS

Patient Population

We recruited 32 patients with known coronary artery disease. Each patient received both PET and SPECT MPI studies within one month. One patient withdrew from the study before completing both sets of images, and two studies were only partially available (one rest listmode file was not saved, one stress injection had inappropriate timing) leaving 29 paired rest/stress and 2 unpaired studies (60 scans in total). The average patient age was 64 ± 11 years and the mean body-mass index was 27.9 ± 4.7 kg/m^2. Twenty-seven (87%) of the patients were male and 6 (19%) had diabetes mellitus. The study was approved by the Ottawa Health Science Network Research Ethics Board and all patients provided informed written consent.

PET Imaging

PET studies were acquired, using either ^{82}Rb (N=25) or ^{13}N-ammonia (N=6), on a Discovery 690 PET/CT scanner (GE Healthcare) according to our clinical protocol. The activity injected at both rest and stress was 10 MBq/kg (^{82}Rb) or 5 MBq/kg (ammonia). Tracer was delivered mechanically as a 30 s bolus (^{82}Rb) or as a rapid bolus by hand (ammonia). MBF was based on data acquired over 8 min (^{82}Rb) or 4 min (ammonia). Stress was induced using dipyridamole (0.14 mg/kg/min for 5 min). Motion correction

was applied as described for the SPECT studies. Kinetic analysis was performed using FlowQuant™ software with a 1-tissue-compartment model and dual-spillover correction as per our clinical protocol (*18*).

SPECT Image Acquisition

SPECT data were acquired in listmode using the Discovery NM530c cardiac camera. Rest images were obtained for 11 min starting immediately prior to injection of 316 ± 71 MBq of ^{99m}Tc-tetrofosmin (Fig. 1). The patient returned at 45 min post-injection for a 5 min static resting acquisition (corresponding to the standard time for MPI). Without repositioning, the patient was stressed using dipyridamole (0.14 mg/kg/min for 5 min) with 11 min of listmode data acquired starting immediately prior to the injection of 1122 ± 170 MBq of tetrofosmin. Both rest and stress injections were delivered mechanically over 30 s. Finally, a standard set of stress perfusion images was acquired at 45 min after tracer injection. The order of PET and SPECT scanning was based on camera availability. The average difference in acquisition dates was 19 ± 9 days with 12 (39%) of the SPECT images obtained prior to PET imaging.

SPECT Image Processing

Similar to our previous animal work (*13*), listmode data were rebinned into a dynamic series of projections (9 x 10 s, 6 x 15 s, 4 x 120 s) and reconstructed using manufacturer supplied iterative reconstruction software (30 iterations), both with and without CT-based AC, followed by Butterworth filtering (order 7, 0.37 cycles/cm). AC used the CT map acquired during PET/CT imaging, which was manually aligned with the SPECT image using on-line quality assurance tools (*13,19*). Kinetic analysis was performed using FlowQuant™ software (*18*) and applying a 1-tissue-compartment model with spill-over correction from blood to myocardium only. The stress dynamic image series was corrected for residual rest activity by subtracting a scaled version of the static rest image acquired just prior to injection of dipyridamole. Analysis was performed with and without BB using the function derived from a porcine model (*13*), and scaled to correct for differences between humans and pigs in the equilibrium plasma-to-whole-blood (*PWB*) concentration (equation 1).

$$PWB(t) = 1.39\, e^{-0.064(t+2.12)^2} + 1.49\, e^{-0.24(t+2.12)} \qquad \text{Eq. 1}$$

where t is time (minutes). In addition, images were processed with and without MC where each dynamic frame was visually compared, in mid-ventricular coronal, sagittal, and transverse planes to a contour outlining the heart in the final frame. The contour was adjusted using a manually defined count threshold to align with the myocardial edge. A rigid-body translation (without rotation) was applied frame-by-frame as needed to center the activity within the contour.

The global left ventricular (LV) K1 values were fit to the PET plasma flow (MBF x (1-hematocrit)), or MBF if a blood-binding correction was not performed, using the Renkin-Crone model (parametrized by α and β, Eq. 2) and a non-linear least squares fitting algorithm.

$$K1 = MBF\left(1 - e^{-(\alpha\, MBF+\beta)/MBF}\right) \qquad \text{Eq. 2}$$

The model fit, accuracy of conversion of SPECT K1 to MBF, and corresponding sensitivity, specificity, and A_{ROC} for an abnormal PET global MFR of < 2.0 (*5*) were assessed using 50 repeats of 2-fold cross-validation (*20*). For 2-fold cross-validation, the patients are randomly divided into two groups. One group is used to estimate the model fit parameters, and the other group is used to test the fitted model's accuracy and vice versa giving two estimates of the model fit parameters and two evaluations of accuracy. Fifty repetitions of the process generates 100 sets of model parameters with associated accuracy measures. For each parameter or measure, the mean and standard deviation (SD) of the 100 values give the overall estimate for the value and its uncertainty. The mean fit parameters were used to calculate the MBF and MFR in each coronary artery territory (regional MBF and MFR) and a similar analysis was performed.

Differences in mean values were compared using paired t-tests and differences in variances with F-tests. A_{ROC}s were calculated non-parametrically with the trapezoidal rule and regional A_{ROC} were compared based on the Mann-Whitney U-statistic (DeLong approach) (*21*). $P < 0.05$, adjusted using a Bonferroni correction for multiple comparisons (n = 12) to $p<0.004$, was considered significant.

RESULTS

The patient characteristics and relationship between SPECT K1 and PET MBF were similar for both PET tracers (Supplemental Fig. 1, Supplemental Tables 1 and 2) and so the data were pooled. The R^2 of the Renkin-Crone model fit was between 0.61 and 0.75 for all methods (Fig. 2, Table 1), and was improved with +MC by an average of 0.05. +MC significantly increased R^2 over –MC for ±AC+BB and +AC-BB ($p<0.001$ for all), but not for -AC-BB ($p=0.005$). From the cross-validation analysis (Table 1), +MC increased the correlation of SPECT and PET MBF by an average of 0.05 over –MC; the increase was significant for ±AC±BB ($p<0.001$). +MC reduced the SD of the MBF difference in all cases (Table 1, Fig. 3; Supplemental Fig. 2).

The average increase in the R^2 of the model fit due to BB was 0.06 (Table 1; Supplemental Fig. 1) and it was significant for –AC±MC ($p<0.001$) but not for +AC±MC ($p\geq0.007$). The average increase in the correlation between SPECT and PET MBF due to BB was 0.06 and was significantly greater for all cases (±AC±MC, $p\leq0.001$). +BB reduced the SD of the MBF difference. The change in SD was significant in all cases except +AC-MC-BB vs +AC-MC+BB (0.55 vs 0.48, $p=0.006$).

With AC, the R^2 of the model fit was lower than with –AC for ±MC+BB ($p<0.001$) but greater for +MC–BB ($p<0.001$) and similar for –MC–BB (0.63 vs 0.61, $p=0.13$). The correlations between SPECT and PET MBF were on average 0.02 worse for +AC than for –AC. –AC significantly increased the correlation for ±MC+BB ($p<0.001$) but not for ±MC–BB ($p>0.02$). +AC did not significantly change the mean or SD of the MBF difference (Fig. 3) except for the SD with -AC+MC+BB vs +AC+MC+BB (0.32 vs 0.37, $p=0.0001$).

The slopes and intercepts of the linear fits between SPECT and PET MBF were within one SD of 1.0 and zero respectively and were not significantly different (Supplemental Table 3). The changes in MBF relative differences (difference / mean) were similar to those for MBF difference (Table 1).

The global SPECT MFR from the cross-validation analysis (Fig. 3; Supplemental Fig. 2, Supplemental Table 4) had an A_{ROC} (Fig. 4) that ranged from 0.87 to 0.98 (Table 2). +MC consistently increased A_{ROC} but the change was only significant for –AC+MC–BB vs –AC–MC–BB (0.98 vs 0.88, p<0.001). +BB increased A_{ROC} for –AC–MC (0.93 vs 0.88, p<0.001) but decreased A_{ROC} for –AC+MC (0.95 vs 0.98, p<0.001) and caused no significant changes for +AC±MC. A_{ROC} was consistently lower with +AC than –AC with the changes all significant except for –MC–BB (p=0.19). Choosing an operating point that gave the highest sensitivity-specificity product yielded sensitivity between 78% and 100% and a specificity between 70% and 100% (Table 2). Similar results were found for stress MBF (Supplemental Fig. 3 and Supplemental Table 5).

Considering regional MBF, there were no statistically significant differences in the correlations between SPECT and PET for any individual pair of correction combinations (Table 3). However, in all cases, +MC had a higher correlation than the corresponding –MC (average difference of 0.06), +BB had a higher correlation than –BB (average difference of 0.07) and +AC had a higher correlation than –AC (average difference of 0.09). The highest correlation was r=0.85, for +AC+MC+BB. The mean residual difference between regional SPECT MBF and PET MBF (Fig. 5) was not significantly different for any pair of correction combinations, except +AC+MC+BB vs –AC+MC+BB (0.05 vs -0.03, p<0.001). The SD in the fit residual consistently decreased with +MC, +BB, and +AC with some differences reaching statistical significance (Table 3). The regional MFR values, determined based on the mean Renkin-Crone model parameters (Table 1), gave consistently higher A_{ROC} with +MC and +BB, but consistently lower A_{ROC} with +AC. However, none of the differences in A_{ROC} were statistically significant. For +AC+MC+BB, A_{ROC} was 0.84 with 70% sensitivity and 86% specificity. For –AC+MC+BB, A_{ROC} was 0.87 with 78% sensitivity and 80% specificity.

DISCUSSION

Our study showed that global MBF measurements with SPECT (±AC+MC+BB), using a solid-state cardiac camera, correlated very well (r = 0.85 to 0.89) with PET MBF measured in the same patients. Our results agreed with an earlier study that correlated a SPECT flow index with ammonia PET MBF (*17*). Our study extended the previous work by determining a suitable extraction fraction correction to convert K1 to an actual measurement of MBF. In addition, we found that global MBF accuracy was improved with MC and BB but not with AC. Our data showed a mean residual difference in SPECT and PET MBF of 0.06 ± 0.37 ml/min/g with all corrections. The sensitivity and specificity for detection of abnormal PET MFR was 100 % and 80% respectively with an A_{ROC} of 0.95 (with -AC+MC+BB). Thus SPECT global MBF may provide additional clinical diagnostic and prognostic benefit compared to relative MPI, similar to PET, despite its reduced spatial resolution, sensitivity and tracer extraction fraction. Although similar overall, there were instances of substantial difference between SPECT and PET MBF (Figs. 3 and 6). The value of SPECT MBF to the interpretation of individual cases will depend on its repeatability which has yet to be evaluated. Evaluation of the incremental clinical value of measuring MBF and MFR with SPECT, and determination of optimal thresholds for normal measurements, will require further studies in a larger patient population.

Motion correction was found to consistently increase both the R^2 of the Renkin-Crone model fit and the correlation between SPECT and PET MBF (Table 1). These results are consistent with previous PET MBF motion studies that showed errors as large as 240% in MBF (*22*) and for which MC improved accuracy (*22,23*). In our work, the reconstructed images were shifted to reduce frame-to-frame motion, but the attenuation map was not re-aligned to correct for motion-induced mis-registration errors in the AC. Additional benefit might be obtained if the mis-registration AC errors were also corrected. Cardiac and respiratory motion correction were not performed for either SPECT or PET scans and these corrections may enhance image resolution and further improve MBF measurement accuracy.

Population-based correction for blood-binding produced a consistent increase in the model fit and the correlation between SPECT and PET MBF. The Renkin-Crone model suggests a physiological basis for the function that converts K1 to MBF. However, as the function parameters are empirically fit, the estimated function can also compensate for other factors, such as BB, inherent in the data. For example, MBF measured using TOF PET with model parameters based on non-TOF PET studies led to a 12% change in the MBF values (*24*). Recalibrating the model parameters leads to an improvement in the MBF values (*25,26*). The different Renkin-Crone parameters given in Table1 reflect the incorporation of different factors such as tracer-blood binding into the empirical K1-to-MBF function, and not changes in physiology. However, forcing these corrections into the form of the Renkin-Crone model may not provide as accurate a compensation as applying the corrections to the images themselves. A closer examination of cases with larger differences between the +BB and -BB results showed that the number of regions with unphysiological values (MFR < 0.9 or > 5) was greater for example with -AC+MC-BB (12/87) than for -AC+MC+BB (3/87). Exclusion of the unphysiological regions, such as was done in (*17*), might improve the MBF and MFR correlations but also sacrifices information from those cardiac segments. There is limited human data on the Renkin-Crone parameters for tetrofosmin, but the 95% confidence intervals for the parameters in Table 1 overlap with those from the study by Shrestha et al (10) and animal studies (13) (Supplemental Fig. 4, Supplemental Table 6).

Finally, AC was evaluated because most SPECT MPI studies are acquired without concurrent transmission imaging. Also, AC increases image noise, partly offsetting the gains in bias achieved through decreased regional heterogeneity. Different approaches to compensating for a lack of AC have been suggested: either restricting measurement to the MFR wherein the ratio compensates for regional attenuation effects (*14,16*), or normalizing so that resting MBF has a predefined population value (*15*). Our data suggest that an appropriate K1-to-MBF conversion function may allow calculation of true global MBF even in the absence of AC. Similar to studies with PET (*27*), our results indicated no consistent benefit to AC in the accuracy of global MBF or A_{ROC}. The myocardial tissue time-activity curve is a convolution of K1 with the arterial input function (18). Thus, because the average attenuation for the myocardium and the input function are similar, the global attenuation effects are largely cancelled out. There may, nevertheless, still be variability in regional MBF due to regional heterogeneity in the myocardial attenuation. Indeed, with regional MBF, AC consistently increased the correlation with PET MBF and consistently decreased the SD of the residuals (Table 3), suggesting that AC improves regional MBF estimation. However, as MFR is a ratio, it provides additional compensation for regional changes in attenuation and consequently, the A_{ROC} for detecting abnormal MFR from the regional analysis also

shows no benefit from AC. One limitation of this study is that the CT scan used for AC was acquired during PET/CT imaging on a separate day and this may have reduced the accuracy of the SPECT AC. A CT acquired in conjunction with the SPECT study might have improved coregistration and so increased the benefit of AC for measuring MBF, but confirming this would require further investigation.

The SPECT activity injected in this study corresponds to a patient radiation dose of 10 mSv (*28*). At this dose, the SPECT time-activity curves were similar in shape but noisier than the PET time-activity curves (Supplemental Fig. 5). Pig studies suggest that reducing the injected activity may be possible (*29*), but further human studies are needed to determine the extent to which patient dose can be reduced while maintaining an accurate MBF estimate. In addition to higher noise, tetrofosmin has a lower extraction fraction at high MBF which reduces the contrast in K1 between normal and abnormal flow responses. Techniques which reduce the uncertainties in kinetic parameter estimation, such as the 4D reconstruction approaches proposed for dynamic imaging with conventional gamma cameras (*10*), might improve MBF estimation with dedicated cardiac SPECT systems, but evaluation of these algorithms will require additional studies. A further consideration in our study is that most of our subjects' PET MBF was done with ^{82}Rb which, although used more commonly in the clinic, has a reduced extraction fraction at high MBF compared to ammonia. Both ammonia and ^{82}Rb have similar diagnostic accuracy (*3*) but uncertainties in the PET flow measurement may have reduced the measured accuracy of the SPECT MBF. Despite similar clinical performance between tetrofosmin and sestamibi, our results cannot be directly extended to sestamibi as we are unaware of any data confirming the extraction fraction function for sestamibi in humans. A final consideration is that the camera's small field of view requires care in patient positioning to avoid truncation of the myocardium.

CONCLUSION

Measuring MBF and MFR in humans is feasible using a dedicated cardiac SPECT camera. Corrections for motion and tracer-blood binding improved global MBF correlation and precision with PET MBF. Global MBF and detection of abnormal MFR were not significantly improved with +AC. With all corrections, SPECT global MBF and MFR differed from PET by 2% ± 32% (MBF) and 2% ± 28% (MFR).

ACKNOWLEDGMENTS

This study was supported by a research operating grant from GE Healthcare.

REFERENCES

1. Camici PG, Rimoldi OE. The clinical value of myocardial blood flow measurement. *J Nucl Med.* 2009;50:1076-1087.

2. Gould KL, Johnson NP, Bateman TM, et al. Anatomic versus physiologic assessment of coronary artery disease: role of coronary flow reserve, fractional flow reserve, and positron emission tomography imaging in revascularization decision-making. *J Am Coll Cardiol.* 2013;62:1639-1653.

3. Schindler TH, Quercioli A, Valenta I, Ambrosio G, Wahl RL, Dilsizian V. Quantitative assessment of myocardial blood flow - clinical and research applications. *Semin Nucl Med.* 2014;44:274-293.

4. Herzog BA, Husmann L, Valenta I, et al. Long-term prognostic value of ^{13}N-ammonia myocardial perfusion positron emission tomography added value of coronary flow reserve. *J Am Coll Cardiol.* 2009;54:150-156.

5. Ziadi MC, Dekemp RA, Williams KA, et al. Impaired myocardial flow reserve on rubidium-82 positron emission tomography imaging predicts adverse outcomes in patients assessed for myocardial ischemia. *J Am Coll Cardiol.* 2011;58:740-748.

6. Murthy VL, Naya M, Foster CR, et al. Improved cardiac risk assessment with noninvasive measures of coronary flow reserve. *Circulation.* 2011;124:2215-2224.

7. 2015 Nuclear medicine market outlook report. IMV Medical Information Division, Des Plaines, IL, 2015.

8. 2015 PET imaging market summary report. IMV Medical Information Division, Des Plaines, IL, 2015.

9. Hsu B, Chen F-C, Wu T-C, et al. Quantitation of myocardial blood flow and myocardial flow reserve with (99m)Tc-sestamibi dynamic SPECT/CT to enhance detection of coronary artery disease. *Eur J Nucl Med Mol Imaging.* 2014;41:2294–2306.

10. Shrestha U, Sciammarella M, Alhassen F. Measurement of absolute myocardial blood flow in humans using dynamic cardiac SPECT and 99mTc-tetrofosmin: method and validation. *J Nucl Cardiol*. 2017;24:268–77.

11. Slomka PJ, Patton JA, Berman DS, Germano G. Advances in technical aspects of myocardial perfusion SPECT imaging. *J Nucl Cardiol.* 2009;16:255-276.

12. Bocher M, Blevis IM, Tsukerman L, Shrem Y, Kovalski G, Volokh L. A fast cardiac gamma camera with dynamic SPECT capabilities: design, system validation and future potential. *Eur J Nucl Med Mol Imaging.* 2010;37:1887-1902.

13. Wells RG, Timmins R, Klein R, et al. Dynamic SPECT measurement of absolute myocardial blood flow in a porcine model. *J Nucl Med.* 2014;55:1685–1691.

14. Ben-Haim S, Murthy VL, Breault C, et al. Quantification of myocardial perfusion reserve using dynamic SPECT imaging in humans: a feasibility study. *J Nucl Med.* 2013;54:873–879.

15. Ben Bouallègue F, Roubille F, Lattuca B, et al. SPECT myocardial perfusion reserve in patients with multivessel coronary disease: correlation with angiographic findings and invasive fractional flow reserve measurements. *J Nucl Med.* 2015;56:1712-1717.

16. Shiraishi S, Sakamoto F, Tsuda N, et al. Prediction of left main or 3-vessel disease using myocardial perfusion reserve on dynamic thallium-201 single-photon emission computed tomography with a semiconductor gamma camera. *Circ J.* 2015;79:623-631.

17. Nkoulou R, Fuchs TA, Pazhenkottil AP, et al. Absolute myocardial blood flow and flow reserve assessed by gated SPECT with cadmium-zinc-telluride detectors using 99mTc-tetrofosmin: head to head comparison with ^{13}N-ammonia PET. *J Nucl Med.* 2016;57:1887-1892.

18. Efseaff M, Klein R, Ziadi MC, et al. Short-term repeatability of resting myocardial blood flow measurements using rubidium-82 PET imaging. *J Nucl Cardiol.* 2012;19:997-1006.

19. Wells RG, Soueidan K, Vanderwerf K, Ruddya TD. Comparing slow-versus high-speed CT for attenuation correction of cardiac SPECT perfusion studies. *J Nucl Cardiol.* 2012;19:719-726.

20. Kohavi R. A study of cross-validation and bootstrap for accuracy estimation and model selection. *14th International Joint Conference on Artificial Intelligence*. 1995:1137-1143.

21. Vergara IA, Norambuena T, Ferrada E, Slater AW, Melo F. StAR: a simple tool for the statistical comparison of ROC curves. *BMC Bioinformatics.* 2008;9:265.

22. Hunter CRRN, Klein R, Beanlands RS, DeKemp RA. Patient motion effects on the quantification of regional myocardial blood flow with dynamic PET imaging. *Med Phys.* 2016;43:1829.

23. Yu Y, Chan C, Ma T, et al. Event-by-event continuous respiratory motion correction for dynamic PET imaging. *J Nucl Med.* 2016;57:1084-1091.

24. Armstrong IS, Tonge CM, Arumugam P. Impact of point spread function modeling and time-of-flight on myocardial blood flow and myocardial flow reserve measurements for rubidium-82 cardiac PET. *J Nucl Cardiol.* 2014;21:467-474.

25. Germino M, Ropchan J, Mulnix T, et al. Quantification of myocardial blood flow with ^{82}Rb: validation with 15O-water using time-of-flight and point-spread-function modeling. *EJNMMI Res.* 2016;6:68.

26. deKemp RA, Klein R, Beanlands RSB. ^{82}Rb PET imaging of myocardial blood flow—have we achieved the 4 "R"s to support routine use? *EJNMMI Res.* 2016;6:69.

27 Tuffier S, Legallois D, Belin A, et al. Assessment of endothelial function and myocardial flow reserve using 15O-water PET without attenuation correction. *Eur J Nucl Med Mol Imaging*. 2016;43:288-295.

28. Einstein AJ, Moser KW, Thompson RC, Cerqueira MD, Henzlova MJ. Radiation dose to patients from cardiac diagnostic imaging. *Circulation.* 2007;116:1290-1305.

29. Timmins R, Klein R, Petryk J, et al. Reduced dose measurement of absolute myocardial blood flow using dynamic SPECT imaging in a porcine model. *Med Phys.* 2015;42:5075.

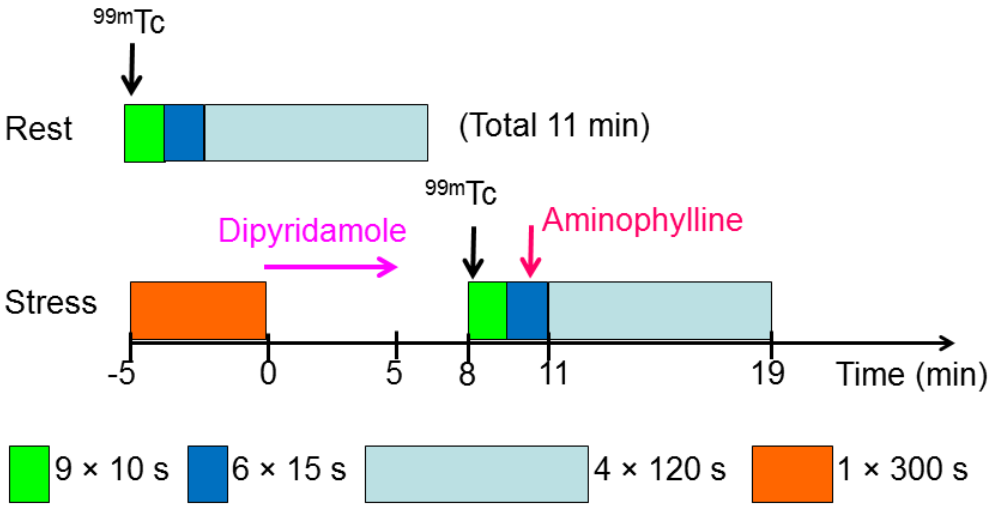

Figure 1: Acquisition protocol for SPECT MBF imaging. Listmode data are acquired for 11 min starting immediately following tracer injection. Data are binned into 9 x 10 s , 6 x 15 s, and 4 x 120 s dynamic frames for reconstruction and analysis.

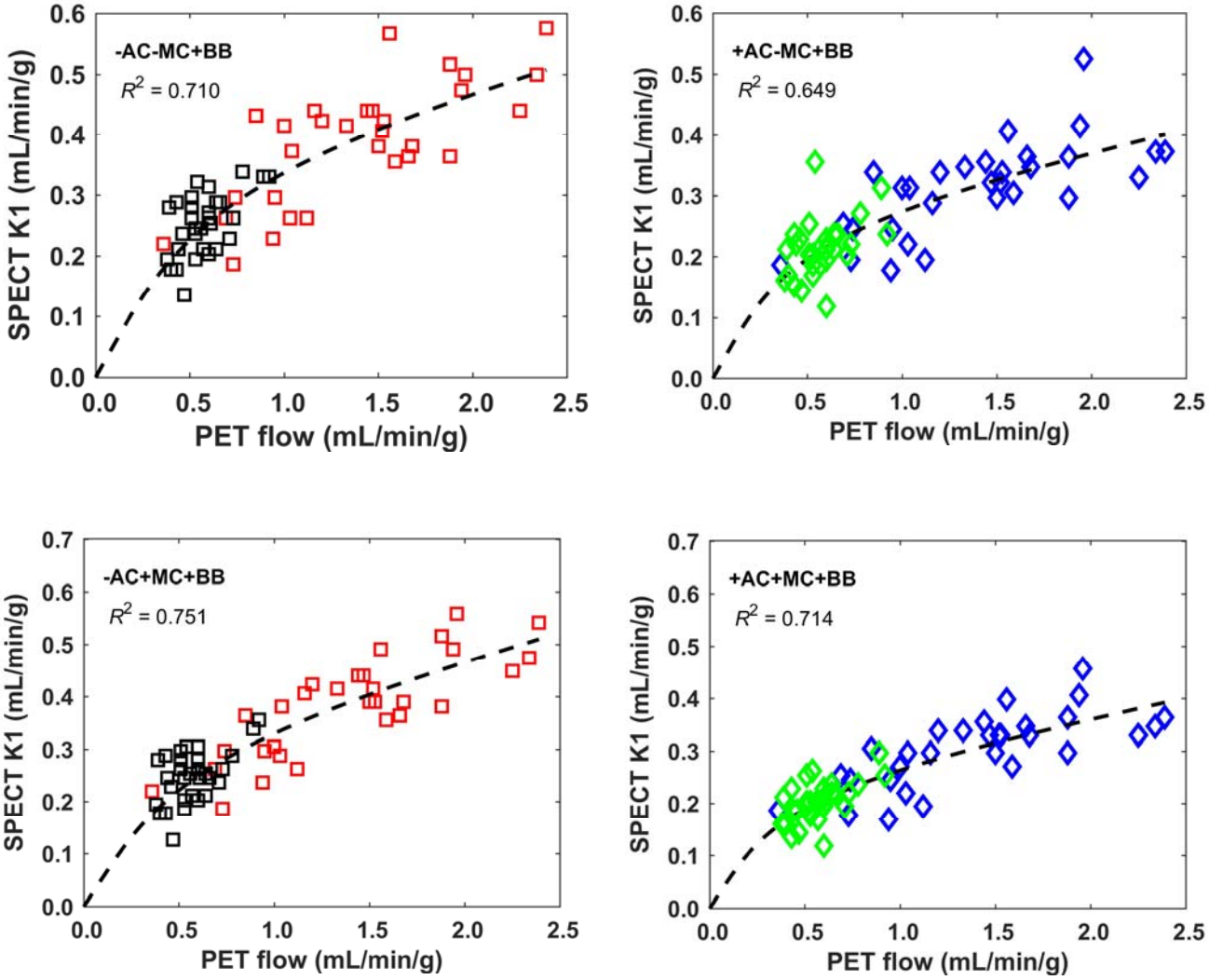

Figure 2: Global SPECT K1 compared to PET MBF, incorporating tracer blood-binding in the kinetic analysis. Results are for data without (-AC) and with (+AC) attenuation correction and without (-MC) and with (+MC) motion corrections. The line gives the mean fit to a Renkin-Crone model for the extraction fraction.

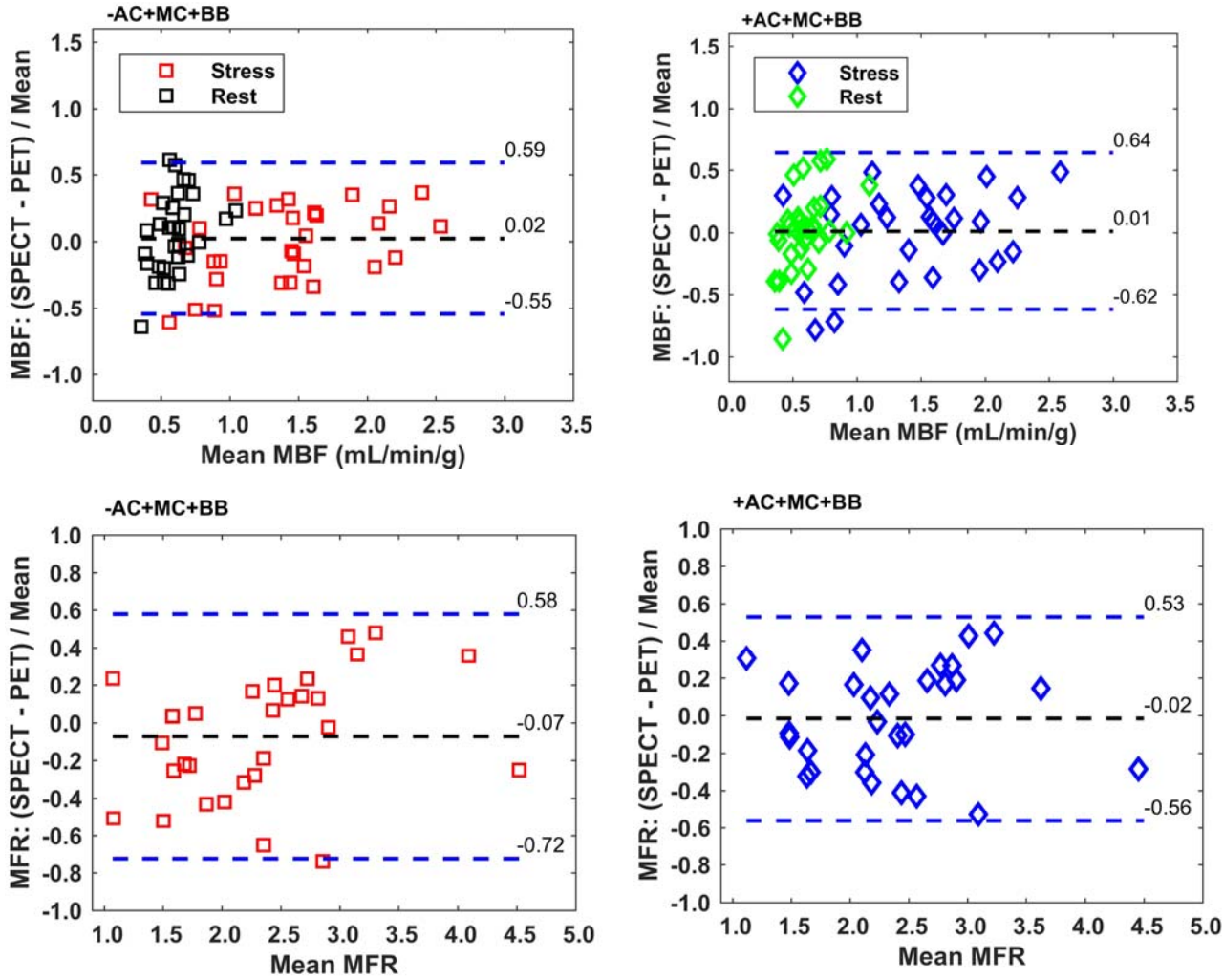

Figure 3: Global SPECT MBF (top) and MFR (bottom) compared to PET, without (-AC) and with (+AC) attenuation correction (N=31 patients (MBF), N=29 patients (MFR)). SPECT MBF values were calculated using the mean of 50-repeat 2-fold cross-validation fit with a Renkin-Crone model for the extraction fraction. MFR is stress MBF / rest MBF. Results are for data without (-AC) and with (+AC) attenuation correction. Both motion and blood-binding corrections were incorporated in all the kinetic analyses. Dashed lines indicate mean and ± 1.96 SD.

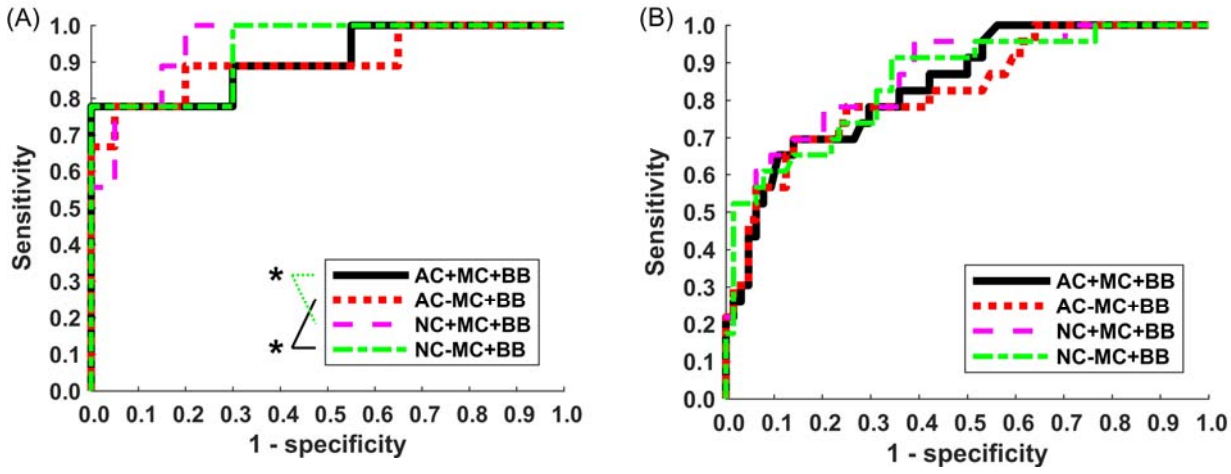

Figure 4: ROC curves for global (A) and regional (B) SPECT MFR compared to abnormal defined as PET MFR < 2. * indicates significantly different A_{ROC}.

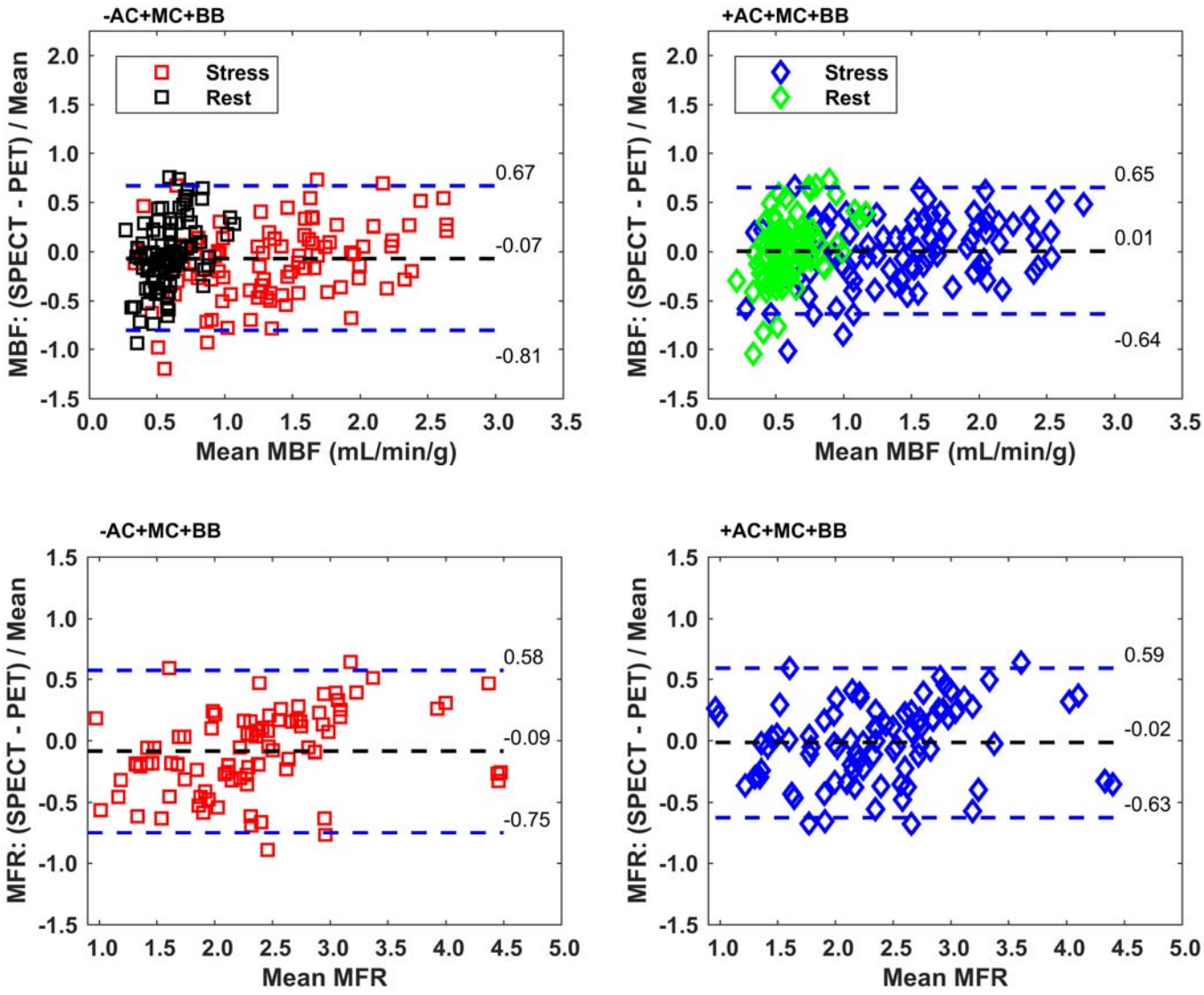

Figure 5: Regional SPECT MBF (top) and MFR (bottom) compared to PET, without (-AC) and with (+AC) attenuation correction (N=180 regions (MBF), 87 regions (MFR)). Motion and blood-binding corrections are applied. Dashed lines indicate mean and ± 1.96 SD.

Table 1: Renkin-Crone model fitting, for images with and without correction of motion (MC), attenuation (AC) and tracer blood binding (BB), and associated fit of SPECT to PET global MBF.

Correction			Renkin-Crone Model[§]			SPECT MBF vs PET MBF				
			R^2	α	β	Correlation R	Difference Mean	Difference SD[¶]	Difference/mean Mean	Difference/mean SD[¶]
-BB	-AC	-MC	0.61[‡]	0.109 ± 0.055	0.731 ± 0.083	0.756[*‡]	0.15	0.61[*‡]	0.05	0.39[*‡]
		+MC	0.65[†‡]	0.114 ± 0.049	0.692 ± 0.079	0.796[*‡]	0.10	0.47[*‡]	0.04	0.35[*‡]
	+AC	-MC	0.63[*]	0.094 ± 0.031	0.516 ± 0.045	0.760[*‡]	0.11	0.55[*]	0.02	0.38[*]
		+MC	0.69[*†]	0.090 ± 0.026	0.496 ± 0.038	0.813[*‡]	0.08	0.44[*‡]	0.02	0.34[*]
+BB	-AC	-MC	0.71[*†‡]	0.158 ± 0.064	0.434 ± 0.054	0.843[*†‡]	0.09	0.41[*‡]	0.03	0.32[*†‡]
		+MC	0.75[*†‡]	0.187 ± 0.055	0.400 ± 0.045	0.885[*†‡]	0.06	0.32[*†‡]	0.03	0.29[*†‡]
	+AC	-MC	0.65[*†]	0.130 ± 0.039	0.308 ± 0.033	0.789[*†‡]	0.09	0.48[*]	0.02	0.36[*†]
		+MC	0.71[*†]	0.140 ± 0.033	0.282 ± 0.027	0.850[*†‡]	0.06	0.37[*†‡]	0.02	0.32[*†]

* +MC vs –MC, $p<0.004$;

† +AC vs –AC, $p<0.004$;

‡ +BB vs –BB, $p<0.004$;

§ Renkin-Crone model: extraction fraction = $1-e^{(-\alpha-\beta/F)}$, F=plasma flow (+BB) or blood flow (-BB). Uncertainties estimated from cross-validation analysis.

¶ SD is mean standard deviation in the MBF difference or difference/mean.

Table 2: Sensitivity, specificity and A_{ROC} for detecting global PET MFR < 2 with SPECT MFR for different correction approaches.

Correction			Global PET MFR < 2 (N=9/29)				
			Threshold[§]	Sens[§]	Spec[§]	Acc[§]	A_{ROC}
-BB	-AC	-MC	2.15	1.00	0.70	0.79	0.882[*‡]
		+MC	1.54	0.89	1.00	0.97	0.975[*†‡]
	+AC	-MC	1.95	0.78	0.90	0.86	0.866
		+MC	1.90	0.78	0.90	0.86	0.878[†]
+BB	-AC	-MC	1.53	0.78	1.00	0.93	0.934[†‡]
		+MC	1.83	1.00	0.80	0.86	0.948[†‡]
	+AC	-MC	1.78	0.78	0.95	0.90	0.897[†]
		+MC	1.70	0.78	1.00	0.93	0.903[†]

* +MC vs –MC for A_{ROC}, p<0.004;

† +AC vs –AC for A_{ROC}, p<0.004;

‡ +BB vs –BB for A_{ROC}, p<0.004;

§ Threshold chosen to maximize Sens x Spec, using mean Renkin-Crone model parameters (Table 1);
Sens=Sensitivity, Spec=Specificity, Acc=Accuracy

Table 3: Linear fit of SPECT to PET regional MBF and resulting sensitivity, specificity and A_{ROC} for detecting regional PET MFR < 2 with SPECT MFR for different correction approaches.

Correction			SPECT MBF vs PET MBF linear fit			Regional PET MFR < 2 (N=23/87)				
			R	Residual	Rel. Diff.	Thresh[§]	Sens[§]	Spec[§]	Acc[§]	A_{ROC}
-BB	-AC	-MC	0.639	0.05 ± 0.65[‡]	-0.05 ± 0.47	1.64	0.65	0.81	0.77	0.800
		+MC	0.668	0.00 ± 0.57[†‡]	-0.08[†] ± 0.45[†]	1.81	0.74	0.78	0.77	0.831
	+AC	-MC	0.742	0.08 ± 0.54[*]	0.00 ± 0.54	2.24	0.74	0.72	0.72	0.770
		+MC	0.816	0.08 ± 0.44[*†]	0.00[†] ± 0.44[†]	2.26	0.78	0.70	0.72	0.780
+BB	-AC	-MC	0.738	0.01 ± 0.49[‡]	-0.04 ± 0.39	2.06	0.91	0.66	0.72	0.850
		+MC	0.780	-0.04[†] ± 0.41[‡]	-0.07[†] ± 0.38	1.79	0.78	0.80	0.79	0.866
	+AC	-MC	0.769	0.07 ± 0.48[*]	0.01 ± 0.37	1.81	0.70	0.86	0.82	0.825
		+MC	0.847	0.05[†] ± 0.37[*]	0.01[†] ± 0.33	1.85	0.70	0.86	0.82	0.841

* +MC vs –MC for R, A_{ROC}, p<0.004;

† +AC vs –AC for R, A_{ROC}, p<0.004;

‡ +BB vs –BB for R, A_{ROC}, p<0.004;

§ Threshold chosen to maximize Sens x Spec, using mean Renkin-Crone model parameters (Table 1);

Sens=Sensitivity, Spec=Specificity, Acc=Accuracy, Rel. Diff. = (SPECT-PET)/Mean

Optimization of SPECT Measurement of Myocardial Blood Flow with Corrections for Attenuation, Motion, and Blood-Binding Compared to PET

R Glenn Wells[1], Brian Marvin[1], Marlie Poirier[1], Jennifer Renaud[1], Robert A deKemp[1], Terrence D Ruddy[1]

[1]Division of Cardiology, University of Ottawa Heart Institute, Ottawa, ON, Canada

SUPPLEMENTARY MATERIAL

SUPPLEMENTARY RESULTS

A breakdown of the patient demographics (Supplemental Table 1), injected tetrofosmin activity and acquisition-date difference between PET and SPECT studies (Supplemental Table 2) showed little difference between the ammonia and rubidium patients. The Rb82 MBF values were originally calibrated against ammonia studies and so the two tracers provide consistent estimates of myocardial blood flow. Thus, it is expected that the relation between SPECT measured K1 values and PET MBF would be consistent between PET tracers and this is what was observed (Supplemental Figure 1). For these reasons, the data from the Rb82 and ammonia patients were pooled together for the analysis presented in this work.

Global K1 values measured with different approaches to the SPECT processing (with and without attenuation correction (AC), with and without motion correction (MC), and with and without tracer-to-blood-binding corrections (BB)) are different, but can all be fit to a process-specific Renkin-Crone model for the extraction fraction function (Supplemental Figure 1). The quality of the fit, as measured by the coefficient of determination (R^2), is improved with MC and with BB, but not with AC.

After converting K1 to MBF with the appropriate extraction fraction correction, the SPECT studies without motion correction (MC) show good correlation with PET MBF (Supplemental Figure 2), but reduced correlation compared to studies with MC (Fig. 3). Correlations between SPECT MFR and PET MFR (Supplemental Figure 2) are similarly reduced compared to images with MC (Fig. 3). The slopes of the linear fit of SPECT MBF to PET MBF are consistently better with +AC, +MC, and +BB, but the differences are not statistically significant (Supplemental Table 3). Similarly, based on the relative difference between SPECT and PET MFR, the MFR showed trends to improvement with +AC, +MC, and +BB, but the differences between correction approaches were not found to be significant (Supplemental Table 4).

SUPPLEMENTARY DISCUSSSION

We note that the majority of patients in this study were male. Gender-based differences have been seen with PET imaging (*30*,*31*) and would also be expected with SPECT, but additional studies with larger numbers of female subjects are needed to confirm this.

The myocardial flow reserve is the most commonly used metric when evaluating absolute flow measurements, but both MFR and one of rest MBF or stress MBF are needed for a complete picture of the heart's function (*2*). Some PET studies have also shown that stress MBF can be a useful indicator of disease (*32*). As a threshold for abnormal stress flow with 82Rb PET, we use 1.2 ml/min/g corresponding to two standard deviations below the mean value for normal subjects (*33*). Using the mean parameters from Table 1 for the Renkin-Crone model to convert stress K1 to MBF, the results are similar to those for MFR (Supplemental Table 5). There is a consistent improvement in the A_{ROC} for BB and MC. With BB and MC, there is similar A_{ROC} for detecting an abnormal PET MBF for both +AC and -AC. Using the DeLong approach to comparing the ROC curves (*21*), we found the AROC for +AC+MC+BB (0.965) was greater than -AC-MC-BB (0.778, p=0.03) and +AC-MC-BB (0.859, p=0.04); -AC+MC+BB (0.954) was greater than -AC-MC-BB (0.778, p=0.04); +AC-MC+BB (0.940) was greater than +AC-MC-BB (0.859, p=0.03); and +AC+MC-BB (0.931) was greater than -AC-MC-BB (0.778, p=0.05). ROC curves are shown for stress MBF in Supplemental Figure 3.

Data are limited on the Renkin-Crone parameters that describe the flow-dependence of the extraction fraction for tetrofosmin. The data are also difficult to compare as the extraction fraction function will depend on the corrections applied to the images during reconstruction and subsequent kinetic analysis. The 95% confidence limits of the values obtained in our study overlap (Supplemental Table 6) with those from a previous study in humans (*10*) and in pigs (*13*), but we note that the uncertainties are relatively large and this can have a substantial impact on the precision of the MBF measurements (*34*). Further studies to refine the parameter measurements would, therefore, be beneficial. We note that there is also an expectation that tetrofosmin would behave similarly to sestamibi. There is good agreement with the values measured in this study and those measured previously in animals (*13*,*35*) for sestamibi (Supplemental Figure 4). Despite the similarity in clinical performance between sestamibi and tetrofosmin, the results of our work cannot be extended directly to studies with sestamibi as there is not any data that we are aware of regarding confirmation of the extraction fraction function for sestamibi in humans.

Representative time-activity curves (TAC) from a stress SPECT and corresponding stress PET Rb82 study are shown in Supplemental Figure 5, along with associated polar map representations of the relative uptake and K1 or Flow distributions. The SPECT data show similar, though noisier, TAC and similar tracer distributions.

The measured myocardial TAC ($C_{myo}(t)$) contains both myocardial tissue and blood contributions due to partial volume effects and the presence of blood vessels in the myocardium.

$$C_{myo}(t) = FBV\ C_b(t) + (1\text{-}FBV)\ C_t(t)$$

where $C_b(t)$ is the blood TAC, $C_t(t)$ is the myocardial tissue TAC, and FBV is the fractional blood volume (*18*). FBV is an additional parameter which is fit during the kinetic analysis. As expected, the reduced

spatial resolution of SPECT compared to PET results in an increase in the mean FBV (Supplemental Table 7). The increased mixing of blood in the $C_{myo}(t)$ signal also suggests that implementing the dual-spillover correction (*18*), as is done in PET, may be beneficial for SPECT MBF measurement.

SUPPLEMENTAL REFERENCES

30. Danad I, Raijmakers PG, Appelman YE, et al. Coronary risk factors and myocardial blood flow in patients evaluated for coronary artery disease: a quantitative [15O]H2O PET/CT study. *Eur J Nucl Med Mol Imaging*. 2012;39:102-112.
31. Duvernoy CS, Meyer C, Seifert-Klauss V, Dayanikli F, Matsunari I, Rattenhuber J, Höss C, Graeff H, Schwaiger M. Gender differences in myocardial blood flow dynamics: lipid profile and hemodynamic effects. *J Am Coll Cardiol*. 1999;33:463-470.
32. Danad I, Uusitalo V, Kero T, et al. Quantitative Assessment of Myocardial Perfusion in the Detection of Significant Coronary Artery Disease: cutoff values and diagnostic accuracy of quantitative [^{15}O]-H2O PET imaging". *J Am Coll Cardiol*. 2014; 64:1464-1475.
33. Lortie M, Beanlands RS, Yoshinaga K, Klein R, Dasilva JN, DeKemp RA. Quantification of myocardial blood flow with 82Rb dynamic PET imaging. *Eur J Nucl Med Mol Imaging*. 2007;34:1765-1774.
34. Moody JB, Murthy VL, Lee BC, Corbett JR, Ficaro EP. Variance Estimation for Myocardial Blood Flow by Dynamic PET. *IEEE Trans Med Imaging*. 2015;34:2343-2353.
35. Leppo JA, Meerdink DJ. Comparison of the myocardial uptake of a technetium-labeled isonitrile analogue and thallium. *Circ Res*. 1989;65:632-639.

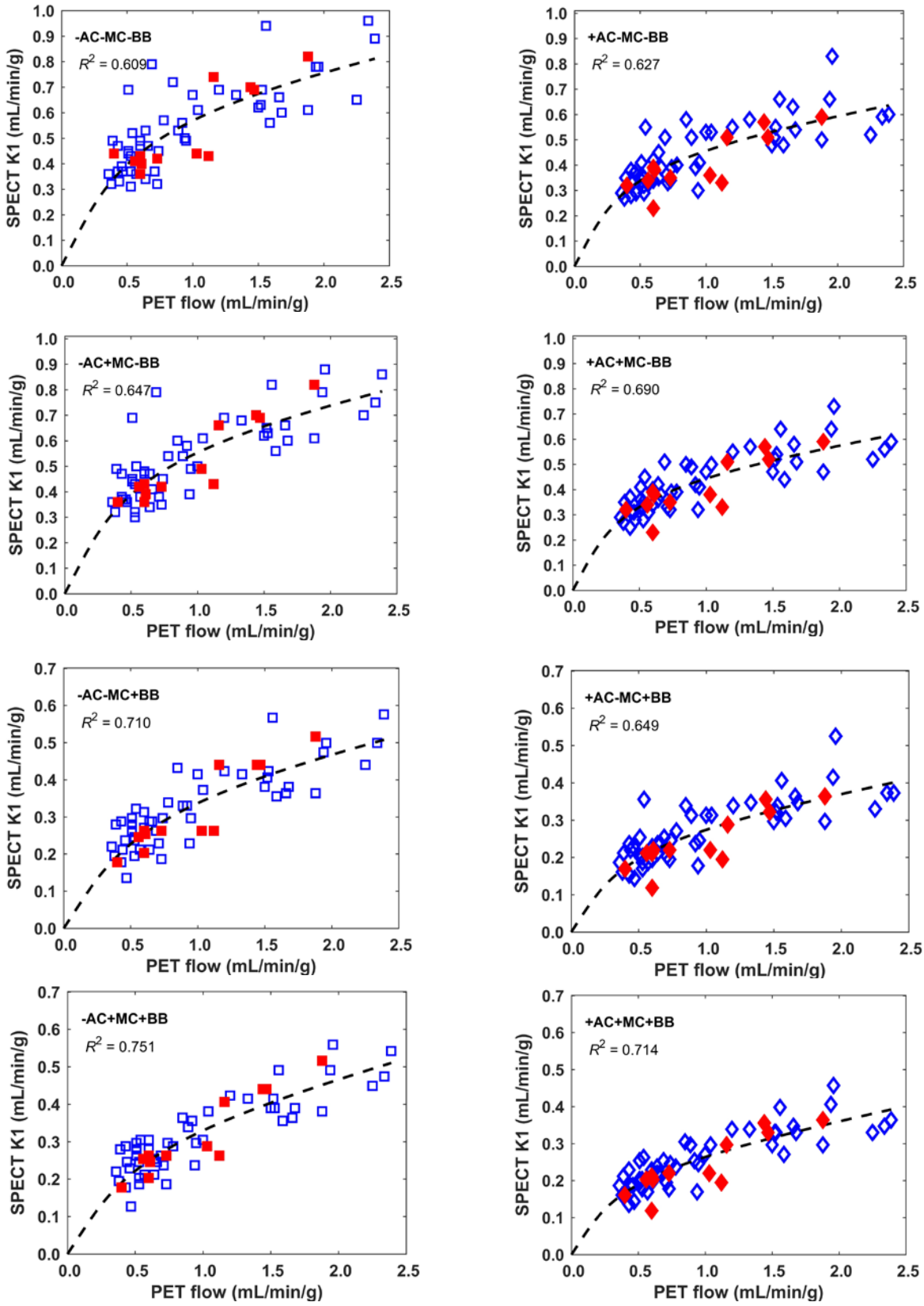

Supplemental Figure 1: Ammonia versus ^{82}Rb. Scatter plots of global SPECT K1 vs PET MBF for different combinations of attenuation (AC), motion (MC), and tracer-to-blood-binding (BB) corrections show the ^{82}Rb data in blue (open) and the ammonia data in red (filled). The scatter of the ammonia data generally falls within that of the ^{82}Rb data and so the data were pooled for analysis. The Renkin-Crone model fit of SPECT K1 and PET flow is shown as a solid line.

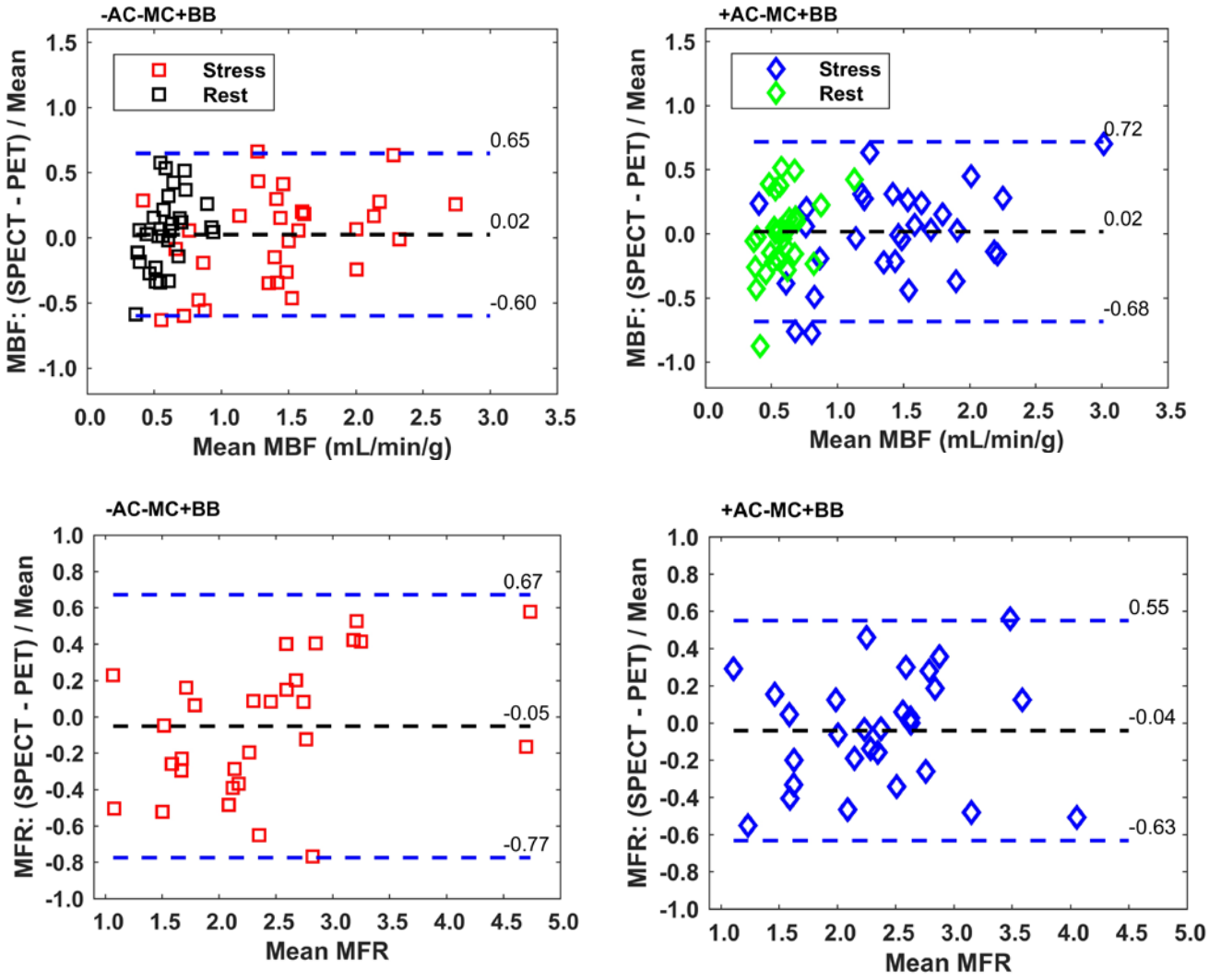

Supplemental Figure 2: Global SPECT MBF (top) and MFR (bottom) compared to PET, without (-AC) and with (+AC) attenuation correction (N=31 patients (MBF), N=29 patients (MFR)). SPECT MBF values were calculated using the mean of 50-repeat 2-fold cross-validation fit with a Renkin-Crone model for the extraction fraction. MFR is stress MBF / rest MBF. Shown are results for images without (-AC) and with (+AC) attenuation correction and without motion corrections. A blood-binding correction was incorporated in all the kinetic analyses. Dashed lines indicate mean and ± 1.96 SD.

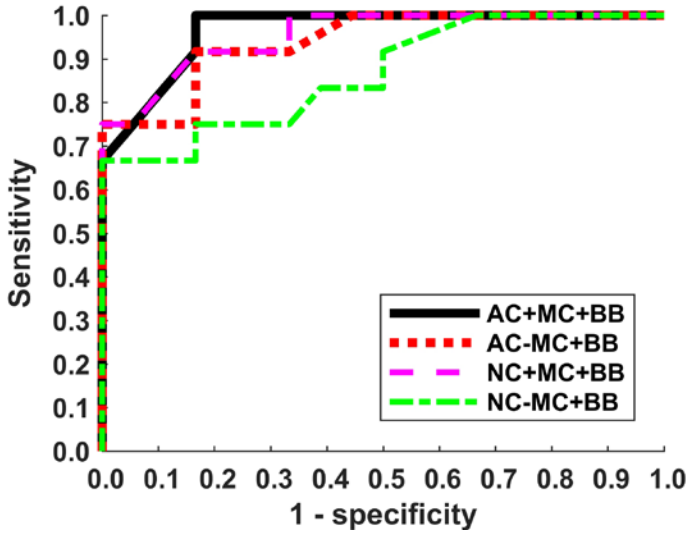

Supplemental Figure 3: ROC curve for detecting an abnormal PET stress MBF (<1.2 ml/min/g) using SPECT stress MBF. There were 12/30 abnormal PET stress MBF cases.

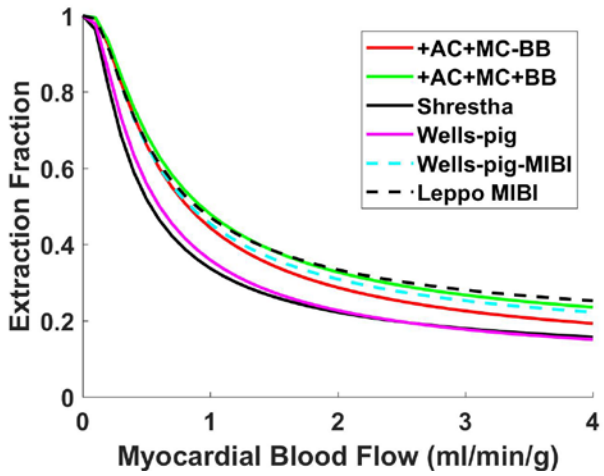

Supplemental Figure 4: Comparison of extraction fractions corresponding to the Renkin-Crone model parameters given in Supplemental Table 5, assuming a human hematocrit of 0.45. The tracer is tetrofosmin in all cases except those labeled with MIBI, which correspond to sestamibi.

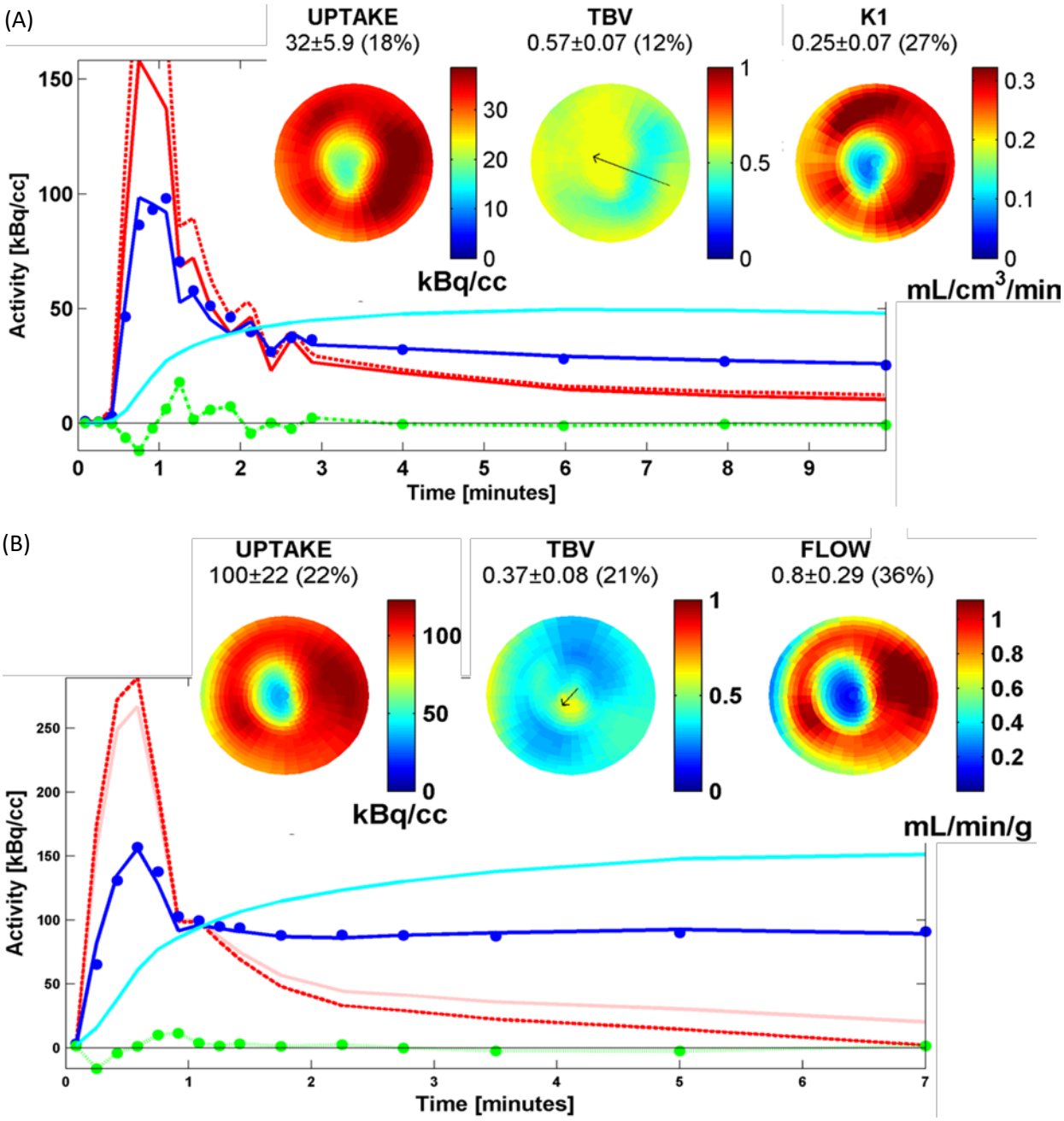

Supplemental Figure 5: Example time-activity curves with associated polar maps from a stress SPECT (A) acquisition and corresponding stress PET scan (B). SPECT time-activity curves (TAC) are similar to but noisier than the PET TAC. Distribution of tracer in the uptake polar maps and also between the SPECT K1 polar map and the PET FLOW polar map. Values indicated for Uptake, fractional blood volume (TBV), K1, and Flow are the mean and standard deviation of those values over 75% of the maximum value.

Supplemental Table 1: Patient Demographics, divided by PET tracer.

	Rb82 (N=25)	NH3 (N=6)	All (N=31)
Male # (%)	22 (88)	5 (83)	27 (87)
Age (years)	65 ± 11	63 ± 12	64 ± 11
BMI (kg/m2)	25.8 ± 3.6	31.0 ± 4.7	27.9 ± 4.7
Diabetes Mellitus # (%)	5 (20)	1 (17)	6 (19)

Supplemental Table 2: Injected tetrofosmin activities and difference in acquisition dates (PET-SPECT).

	Rb82 (N=25)	NH3 (N=6)	All (N=31)
Rest (MBq)	307 ± 65	345 ± 88	316 ± 70
Stress (MBq)	1094 ± 170	1195 ± 161	1122 ± 170
Acquisition date difference (days)	20 ± 9	15 ± 10	19 ± 9
SPECT before PET # (%)	9 (36)	3 (50)	12 (39)

Supplemental Table 3: Slopes and intercepts for linear fits of SPECT MBF to PET MBF from cross-validation analysis (global) and from using the mean Renkin-Crone parameters for conversion (regional).

Correction			Global		Regional	
			Slope	Intercept	Slope	Intercept
-BB	-AC	-MC	1.19	-0.03	0.92	0.13
		+MC	1.07	0.03	0.87	0.13
	+AC	-MC	1.10	0.02	1.02	0.06
		+MC	1.06	0.02	1.06	0.02
+BB	-AC	-MC	1.09	0.00	0.92	0.09
		+MC	1.03	0.02	0.86	0.10
	+AC	-MC	1.05	0.04	0.99	0.08
		+MC	1.03	0.04	1.00	0.04

Supplemental Table 4: Comparison of SPECT and PET MFR.

Correction			SPECT MFR – PET MFR			
			Global Difference/ Mean		Regional Difference/ Mean	
			Mean	SD§	Mean	SD§
-BB	-AC	-MC	-0.03	0.47	-0.04	0.49
		+MC	-0.05	0.41	-0.05	0.43
	+AC	-MC	-0.02	0.35	-0.02	0.40
		+MC	-0.01	0.32	0.01	0.37
+BB	-AC	-MC	-0.05	0.37	-0.07	0.38
		+MC	-0.07	0.33	-0.09	0.34
	+AC	-MC	-0.04	0.30	-0.05	0.34
		+MC	-0.02	0.28	-0.02	0.31

* +MC vs –MC, p<0.004;

† +AC vs –AC, p<0.004;

‡ +BB vs –BB, p<0.004;

§ SD is standard deviation in the MFR difference/mean.

Supplemental Table 5: Sensitivity, specificity and area under the receiver-operating-characteristic curve (A_{ROC}) for detecting global PET stress MBF < 1.2 with SPECT stress MBF for different corrections.

Correction			Global PET stress MBF < 1.2 (N=12/29)				
			Threshold§	Sens§	Spec§	Acc	A_{ROC}
-BB	-AC	-MC	0.86	0.58	1.00	0.83	0.778
		+MC	1.28	0.83	0.83	0.83	0.889
	+AC	-MC	1.53	0.92	0.67	0.77	0.859
		+MC	1.50	1.00	0.78	0.87	0.931
+BB	-AC	-MC	0.95	0.67	1.00	0.87	0.866
		+MC	1.37	0.92	0.83	0.87	0.954
	+AC	-MC	1.46	0.92	0.83	0.87	0.940
		+MC	1.66	1.00	0.83	0.90	0.965

* +MC vs –MC for A_{ROC}, p<0.004;

† +AC vs –AC for A_{ROC}, p<0.004;

‡ +BB vs –BB for A_{ROC}, p<0.004;

§ Threshold chosen to maximize Sens x Spec, using mean Renkin-Crone model parameters (Table 1);
Sens=Sensitivity, Spec=Specificity, Acc=Accuracy

Supplemental Table 6: Comparison of Renkin-Crone model parameters for the extraction fraction

Source	Species	Tracer	α	α 95% CI	β (ml/min/g)	β 95% CI (ml/min/g)
+AC+MC-BB	human	tetrofosmin	0.090	0.039 – 0.141	0.496¶	0.422 – 0.570
+AC+MC+BB	human	tetrofosmin	0.140	0.075 – 0.205	0.282	0.229 – 0.335
Wells*	pig	tetrofosmin	0.070	0.041 – 0.099	0206	0.167 – 0.245
Shrestha†	human	tetrofosmin	0.091	-0.105 – 0.287	0.32	0.006 – 0.634
Wells*	pig	sestamibi	0.114	0.051 – 0.215	0.286	0.168 – 0.352
Leppo‡	rabbit	sestamibi	0.175	0.095 – 0.255	0.254	0.162 – 0.346

* Wells et al, *J Nucl Med.* 2014. (*13*)

† Shrestha et al, *J Nucl Cardiol.* 2016. (*10*)

‡ Data refit from Leppo et al, Circ Res. 1989. (*35*)

¶ As the extraction fraction is a function of blood-flow, rather than plasma flow, β for +AC+MC-BB is equivalent to β for +AC+MC+BB times (1-HCT), where HCT is the human hematocrit = 0.45.

Supplemental Table 7: Average Fractional Blood Volume (FBV) measured during kinetic analysis

Method	FBV - rest	FBV - stress
PET	0.31 ± 0.06	0.32 ± 0.07
SPECT (average)	0.42 ± 0.06	0.47 ± 0.06
-AC-MC-BB	0.43 ± 0.05	0.47 ± 0.06
-AC+MC-BB	0.40 ± 0.06	0.45 ± 0.07
-AC-MC+BB	0.44 ± 0.05	0.49 ± 0.05
-AC+MC+BB	0.43 ± 0.06	0.49 ± 0.06
+AC-MC-BB	0.41 ± 0.06	0.45 ± 0.06
+AC+MC-BB	0.39 ± 0.07	0.44 ± 0.07
+AC-MC+BB	0.43 ± 0.06	0.48 ± 0.05
+AC+MC+BB	0.41 ± 0.06	0.46 ± 0.06